Raman spectroscopy and DFT modelling of Tl2S-GeS2 crystals and glasses

M. Bokova, A. Paraskiva, Daniele Fontanari, A. Cuisset, M. Kassem, E. Bychkov

Version of Record: https://www.sciencedirect.com/science/article/pii/S0022309322006494
Manuscript_39575436afddebd391f3b5db883d141c

Raman spectroscopy and DFT modelling of Tl_2S-GeS_2 crystals and glasses

M. Bokova*, A. Paraskiva, D. Fontanari, A. Cuisset, M. Kassem, E. Bychkov

Université du Littoral Côte d'Opale, LPCA, EA 4493, F-59140 Dunkerque, France

*Corresponding author. Laboratoire de Physico-Chimie de l'Atmosphère, Université du Littoral Côte d'Opale, 189A avenue M. Shumann, 59140 Dunkerque, France. Tel.: +33 2 28 65 82 70; fax: +33 3 28 65 82 44.
E-mail address: Maria.Bokova@univ-littoral.fr (M. Bokova)

Keywords

Thallium thiogermanate glasses, Raman spectroscopy, DFT modelling

Abstract

Thallium thiogermanate glasses and crystals were studied by Raman spectroscopy accompanied by DFT modelling. The experimental Raman spectra of the known crystalline compounds in the Tl_2S-GeS_2 system are consistent with the crystal structure and DFT modelling of the respective Tl-Ge-S clusters, representing structural motifs in c-$Tl_4Ge_4S_{10}$, c-$Tl_4Ge_2S_6$, and c-Tl_4GeS_4. The Raman spectra of the $(Tl_2S)_x(GeS_2)_{1-x}$ glasses can be divided into two groups: (1) semiconducting glasses at $x \leq 0.3$, and (2) ion-conducting vitreous alloys at $x > 0.3$. At $x \leq 0.3$, the continuous g-GeS_2 network is transformed into a fragmented structure consisting of adamantane-like units Ge_4S_{10} held together by thallium species. In the ion-conducting composition domain at $x > 0.3$ takes place further fragmentation of tetrahedral tetramers Ge_4S_{10} into edge-sharing ES-Ge_2S_6 dimers and small corner-sharing CS-oligomers, i.e., CS-Ge_2S_7 dimers or CS-Ge_3S_{10} trimers.

1. Introduction

Heavy metal chalcogenide glasses appear to be promising optical materials transparent in far-IR [1-2], highly sensitive membranes for heavy metal ion detection [3-6] and interesting model materials exhibiting heavy ion transport in solids [7-13]. Structural studies of lead, cadmium, mercury or thallium chalcogenide glasses are rather rare, except for a few reports [14-20]. In the $(Tl_2S)_x(GeS_2)_{1-x}$ system, glasses are formed over the entire composition region at $x \leq 0.5$ [13]. It should, however, be noted that thallium-poor glasses, $x \leq 0.15$, show small Bragg peaks in both large neutron and small X-ray samples, which correspond to high-temperature β-GeS_2. A spatial incompatibility between 2D network structure of glassy GeS_2 and isolated tetrahedral Ge_4S_{10} clusters (Fig. 1) seems to be the reason of enhanced crystallization ability of the Tl-poor glasses.

Three ternary compounds are known in the $(Tl_2S)_x(GeS_2)_{1-x}$ system [21-23] in addition to two binary end-members GeS_2 and Tl_2S (Fig. 1). In a remarkable contrast to low-temperature 3D lattice or high-temperature 2D lattice, Fig. 1(d), of the α- and β-GeS_2 polymorphs [24-25], crystalline thallium thiogermanates exhibit isolated Ge-S anions held together by thallium species. Thallium-poor monoclinic $Tl_4Ge_4S_{10}$ (x = ⅓), space group $C2/c$, crystallizes in adamantane-type structure consisting of highly symmetric tetrahedral units Ge_4S_{10} (T_d symmetry), Fig. 1(c) [21]. The corner-sharing CS-$GeSS_{3/2}$ tetrahedra in the adamantane units share their corners and exhibit two types of Ge-S distances for bridging S_b and terminal S_t sulfur species: $r(Ge - S_b)$ = 2.26±0.05 Å and $r(Ge - S_t)$ = 2.141±0.012 Å. The average Ge-Ge distance between neighboring CS-$GeSS_{3/2}$ is 3.58±0.02 Å.

The adamantane-like structural motif is widely adopted by analogous alkali thio- and selenogermanates and silicates (see, for example, [26-28] and references therein). In equimolar compound, triclinic $Tl_4Ge_2S_6$ ($x = \frac{1}{2}$), space group $P\bar{1}$, isolated edge-sharing ES-Ge_2S_6 dimers are found, Fig. 1(b). The Ge-S distances also show a difference between S_b and S_t species: $r(Ge - S_b)$ = 2.274±0.003 Å and $r(Ge - S_t)$ = 2.16±0.02 Å. The Ge-Ge distance in the ES-Ge_2S_6 dimer is 3.074±0.003 Å. Finally, in thallium-rich monoclinic Tl_4GeS_4 (x = ⅔), space group Cc, isolated tetrahedra GeS_4 are held together by thallium ions, Fig. 1(a). The average Ge-S interatomic distance is $r(Ge - S_t)$ = 2.216±0.025 Å. In all three Tl_2S-GeS_2 crystalline compounds the thallium coordination is high, 6 (Tl_4GeS_4) ≤ N_{Tl-S} ≤ 9 ($Tl_4Ge_4S_{10}$), and decreases with x. The average Tl-S interatomic distance also depends on thallium content x: 3.44±0.27 Å (x = ⅓) → 3.11±0.07 Å ($x = \frac{1}{2}$) → 3.02±0.10 Å (x = ⅔).

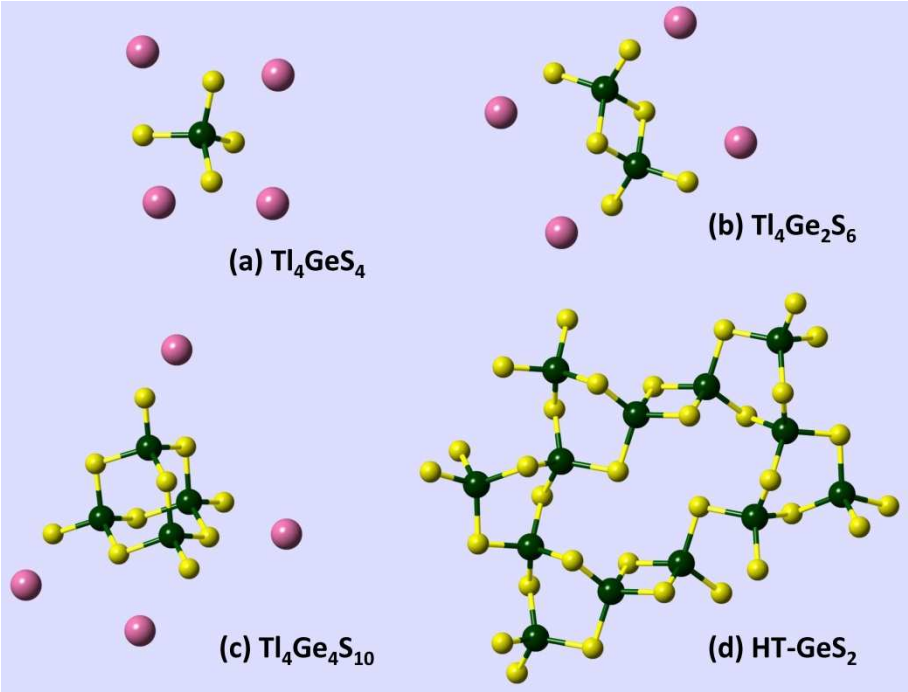

Figure 1. Structural motifs in the Tl_2S-GeS_2 system [21-23]: (a) thallium-rich monoclinic Tl_4GeS_4 (x = ⅔), space group Cc, (b) equimolar triclinic $Tl_4Ge_2S_6$ ($x = \frac{1}{2}$), space group $P\bar{1}$, and (c) thallium-poor monoclinic $Tl_4Ge_4S_{10}$ (x = ⅓), space group $C2/c$. (d) Characteristic layer structure in high-temperature monoclinic modification β-GeS_2, space group $P2_1/c$ [24]. Thallium, germanium and sulfur atoms are presented in pink, green and yellow, respectively.

The goal of the present paper is to unveil the local environment in thallium thiogermanate glasses $(Tl_2S)_x(GeS_2)_{1-x}$, $0 \le x \le 0.5$, compare it with known crystalline references and reveal a difference between semiconducting, $x \le 0.3$, and ion-conducting, $x > 0.3$, vitreous alloys [13]. As a first step, we report here Raman spectroscopy results for the Tl_2S-GeS_2 glasses and crystals accompanied by DFT modelling of the vibrational spectra. Further steps including pulsed neutron diffraction and high-energy X-ray scattering will be reported elsewhere.

2. Material and methods

2.1. Samples preparation

The glassy samples in the $(Tl_2S)_x(GeS_2)_{100-x}$ system, where x = 0, 0.05, 0.1, 0.15, 0.2, 0.3, 04, 0.5 Tl_2S fraction were prepared from high purity elements by the standard melt-quenching technique. $Tl_4Ge_4S_{10}$, $Tl_4Ge_2S_6$ and Tl_4GeS_4 crystals were prepared from its constituents by thermal synthesis in the evacuated silica tube according to the procedure described previously by Eulenberger [21-23]. The details for the glass and crystals synthesis as well as the glass forming region, macroscopic and transport properties of the solids are described in our previous paper [13].

2.2. Raman spectroscopy measurements, Raman data treatment and DFT modelling

The Raman spectra of the glasses were collected on a LABRAM Dilor spectrometer (Jobin Yvon Horiba Group) equipped with a liquid nitrogen cooled CCD detector and a microscope. He–Ne laser operating at an excitation wavelength of 632.8 nm was used. Each spectrum was recorded at room temperature in the 80-1200 cm^{-1} spectral range using a power level of 0.1 mW (to avoid crystallisation of the glassy samples) and a resolution of 1 cm^{-1}. The acquisition time varied between 60 and 150 s. In order to verify the sample homogeneity and the absence of photo-induced phenomena, two to four spectra were registered for each sample at different positions. The measured raw Raman spectra were analysed over the 100–600 cm^{-1} range. The spectral background was approximated by a Voigt function and then subtracted from the experimental data with further normalization to the most intense feature. Typical raw Raman spectra treatment is shown in Fig. S1 (supplementary material).

The DFT calculations have been carried out using GAUSSIAN® 16 [29] software associated with its graphical user interface GaussView® 6.1. Optimisation of the DFT frequency calculations was carried out with the Becke [30] three parameters hybrid exchange functional and the Lee–Yang–Parr correlation functional (B3LYP) [31] associated with 6-311++G(3df,2p) basis-set. In order to find a compromise between the cost of the calculations and the accuracy of the results, structural optimisations and harmonic vibrational frequency calculations were performed for isolated size-limited clusters: GeS_4Tl_4, $Ge_2S_6Tl_4$, $Ge_4S_{10}Tl_4$, $Ge_3S_{10}Tl_8$, $Ge_3S_9Tl_6$, corner-sharing CS-$Ge_3S_{10}Tl_8$ trimer and CS-$Ge_3S_9Tl_6$ ring. All the structures were optimized using the tight convergence option ensuring adequate convergence and reliability of computed wavenumbers. Further details of the DFT simulations are published elsewhere [20] [32].

3. Results and discussion

3.1. Experimental and simulated Raman spectra in the Tl_2S-GeS_2 crystals

The experimental Raman spectra of the synthesized crystalline compounds in the Tl_2S-GeS_2 system are shown in Fig. 2(a). We should note that neither IR nor Raman spectra of crystalline thallium thiogermanates were reported. Consequently, we can only compare the

obtained spectra with similar alkali thiogermanate crystals and carry out a DFT modelling of Tl-Ge-S clusters representing the structural motifs in the Tl_2S-GeS_2 system (Fig. 3).

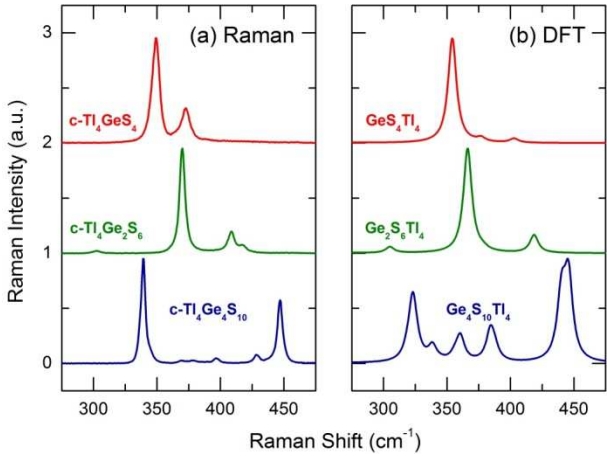

Figure 2. (a) Experimental Raman spectra of the crystalline reference compounds $Tl_4Ge_4S_{10}$ (x = ⅓), $Tl_4Ge_2S_6$ ($x = \frac{1}{2}$), and Tl_4GeS_4 (x = ⅔) within the Ge-S stretching spectral domain, and (b) DFT Raman spectra of the respective Tl-Ge-S clusters.

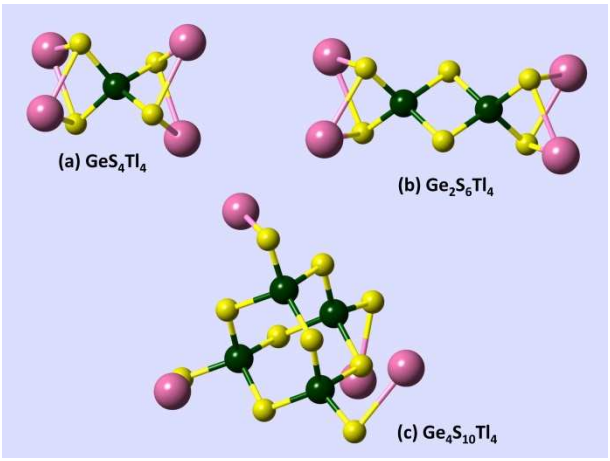

Figure 3. Optimized geometry of the Tl-Ge-S clusters: (a) GeS_4Tl_4, (b) $Ge_2S_6Tl_4$, and (c) $Ge_4S_{10}Tl_4$, used for DFT modelling of vibrational spectra of the crystalline reference compounds Tl_4GeS_4, $Tl_4Ge_2S_6$, and $Tl_4Ge_4S_{10}$, respectively.

The optimized geometry of GeS_4Tl_4, $Ge_2S_6Tl_4$ and $Ge_4S_{10}Tl_4$ clusters (interatomic distances and bond angles) are summarized in Table 1 and compared with crystallographic results [21-23]. The DFT simulations show a good agreement with the crystal structure.

Table 1. Optimized geometry parameters (Ge-S and Tl-S interatomic distances, S-Ge-S, Ge-S-Ge, S-Tl-S and Tl-S-Tl bond angles) of the Tl-Ge-S clusters used for DFT modelling of vibrational spectra in comparison with crystallographic results [21-23].

	Ge-S (Å)	S-Ge-S (deg)	Ge-S-Ge (deg)	Tl-S (Å)	S-Tl-S (deg)	Tl-S-Tl (deg)
GeS_4Tl_4	2.241	110(6)	–	2.956	72.6	90.9
c-Tl_4GeS_4 [23]	2.22(3)	109(2)	–	3.02(10)[a]	73.4(7)	119(14)
$Ge_2S_6Tl_4$	2.25(2)	110(9)	84.4	2.938	72.0	85.4
c-$Tl_4Ge_2S_6$ [22]	2.22(5)	109(7)	85.0	3.11(7)[a]	75(2)	130(31)
$Ge_4S_{10}Tl_4$	2.25(7)	109(5)	108(3)	2.826	–	–
c-$Tl_4Ge_4S_{10}$ [21]	2.22(7)	109(3)	107(2)	3.07(4)[a]	72.0(10)	83.8(4)

[a] The shortest Tl-S interatomic distances. [b] The last digit(s) in parentheses corresponds to the mean-square deviation (MSD) of the average experimental or calculated values. The missing MSD for the calculated geometry parameters means either a single calculated value or a negligible difference between several nearly identical geometry parameters.

$Tl_4Ge_4S_{10}$

The Raman spectrum of the thallium-poor crystal within the Ge-S stretching domain (≈300 ≤ ν ≤ ≈450 cm^{-1}) exhibits two intense vibrational features at 339 and 447 cm^{-1}. Similar spectra were observed for alkali thiogermanate crystals $M_4Ge_4S_{10}$ (M = K, Rb, Cs) [28]; the intense features were attributed to the A_1 vibration modes representing Ge-S stretching of bridging and terminal sulfur species, respectively. Our DFT modelling reproduces rather well the Raman features of $Tl_4Ge_4S_{10}$, Fig. 2(b). The positions of the two most intense A_1 modes are consistent with experimental results. The 339 cm^{-1} mode corresponds to the in-phase breathing of the Ge_4S_{10} tetrahedral cluster. The high-frequency feature at 447 cm^{-1} is related to the in-phase symmetric stretching of the terminal sulfur species. The apparent discrepancy is observed for the amplitudes of multiple asymmetric stretching modes while their positions reflect the experimental features. It is worth mentioning that the calculated DFT intensities are similar to those in heavy alkali analogues of the thallium compound, i.e., $Cs_4Ge_4S_{10}$ or $Rb_4Ge_4S_{10}$ [28]. As expected, the Tl-related vibrations appear at low frequencies, ν < 100 cm^{-1}.

$Tl_4Ge_2S_6$

The agreement between DFT and experimental Raman spectra is better for equimolar $Tl_4Ge_2S_6$ in both peak positions and amplitudes. The most intense feature at 370 cm^{-1} corresponds to the in-phase breathing of the edge-sharing ES-Ge_2S_6 dimer of the A_1 symmetry. The high-frequency mode at 409 cm^{-1} is related to the B_1 in-phase asymmetric stretching of bridging and terminal sulfur atoms. The bending and deformation Ge-S vibrations are observed below 200 cm^{-1}, similar to those in adamantane units. The Tl-related features appear below 100 cm^{-1}, as in $Tl_4Ge_4S_{10}$. There is no available Raman data for similar alkali thiogermanates. The only exception appears to be monoclinic $Na_4Ge_2S_6$ with different crystal structure consisting of infinite (CS-$GeS_2S_{2/2})_\infty$ chains instead of isolated ES-Ge_2S_6 dimers [33]. Consequently, its Raman spectrum [34] looks differently compared to $Tl_4Ge_2S_6$.

Tl_4GeS_4

Finally, the thallium-rich crystal Tl_4GeS_4 also exhibits a good agreement with DFT modelling. The most intense spectroscopic feature at 349 cm^{-1} corresponds to the A_1 breathing of isolated GeS_4 tetrahedra while asymmetric stretching and bending/deformation modes are observed either at higher frequencies or below 230 cm^{-1}, respectively. As expected, the Tl-related modes appear below 100 cm^{-1}.

Resuming, we observe an excellent consistency between the crystal structure of Tl_2S-GeS_2 compounds, their experimental Raman spectra and DFT modelling.

3.2. Experimental Raman spectra in the Tl_2S-GeS_2 glasses

Before discussing the evolution of Raman features in the quasi-binary glassy system, it seems to be reasonable to remind the main structural motifs in glassy g-GeS_2, reflected by their characteristic vibrational modes and DFT replicas [35], shown in Fig. 4.

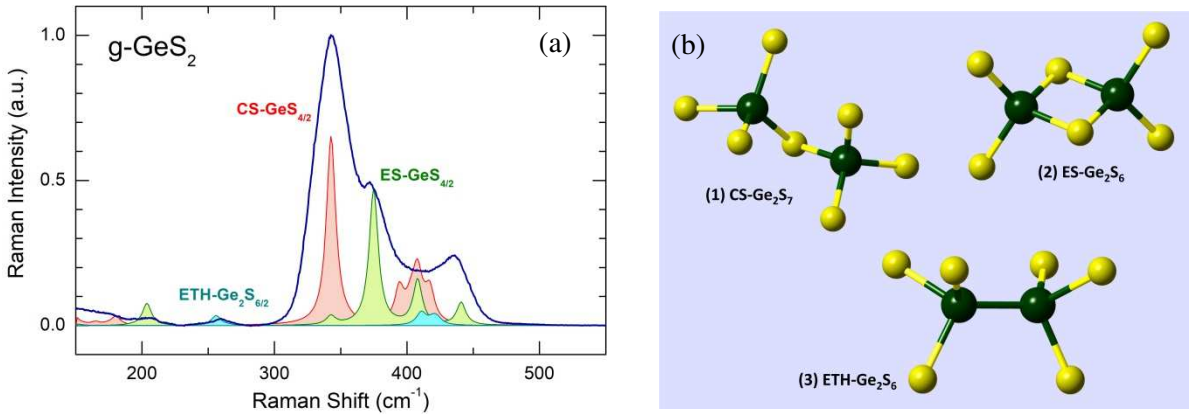

Figure 4. (a) Experimental Raman spectrum of glassy GeS_2 and DFT Raman spectra of corner-sharing CS-$GeS_{4/2}$ and edge-sharing ES-$GeS_{4/2}$ tetrahedra, as well as of ethane-like ETH-$Ge_2S_{6/2}$ units [35]; (b) schematic representation of (1) CS-Ge_2S_7, (2) ES-Ge_2S_6, and (3) ETH-Ge_2S_6 clusters used for DFT modelling. The terminal hydrogen species are not shown and H-related vibrational modes are removed from the DFT spectra.

The GeS_2 stoichiometric glass exhibits well-known spectroscopic features consistent with neutron and X-ray diffraction results (see for example [36-38] and references therein). The most intense line at 344 cm^{-1} correspond to the A_1 symmetric in-phase breathing of corner-sharing CS-$GeS_{4/2}$ tetrahedra [39-41], accompanied by a A_{1c} companion line at 372 cm^{-1} [42] related to the symmetric breathing of edge-sharing ES-$GeS_{4/2}$ units. The broad asymmetric feature at 259 cm^{-1} originates from Ge-Ge stretching in ethane-like ETH-$Ge_2S_{6/2}$ units [42-44]. Recent *ab initio* calculations [35,44,45] have shown that the broad poorly resolved feature around 400 cm^{-1} contains contributions from both CS- and ES-tetrahedra as well as from ETH-units, but the peak at 436 cm^{-1} is due entirely to the highest F_2 mode in the ES-$GeS_{4/2}$ tetrahedra [35,45].

As it was mentioned previously [13], the Tl-poor glasses ($0.05 \leq x \leq 0.15$) are hardly to be obtained without crystalline impurities of high-temperature β-GeS_2. The Raman spectroscopy measurements, Fig. 5, confirm the diffraction results. In particular, for these glass compositions it was possible to find the β-GeS_2 crystallites at the glass surface and collect good quality spectra, Fig. 6(b). The reason of such behavior seems to the difference in crystal structure of β-GeS_2 and Tl-poor $Tl_4Ge_4S_{10}$ (x = ⅓), Fig. 1. The high-temperature β-GeS_2 polymorph consists of 2D layers formed by CS- and ES-$GeS_{4/2}$ tetrahedra forming two-, three- and eight-membered rings. The crystal structure of β-GeS_2 appears to be the main structural motif of glassy GeS_2 [21,35-44]. In contrast, monoclinic $Tl_4Ge_4S_{10}$ consists of isolated adamantane units Ge_4S_{10} connected by thallium species, i.e., its local and intermediate-range order is drastically different from that in β- and glassy GeS_2. Consequently, the spatial incompatibility of the structural motifs leads to enhanced crystallization ability of the Tl-poor glasses.

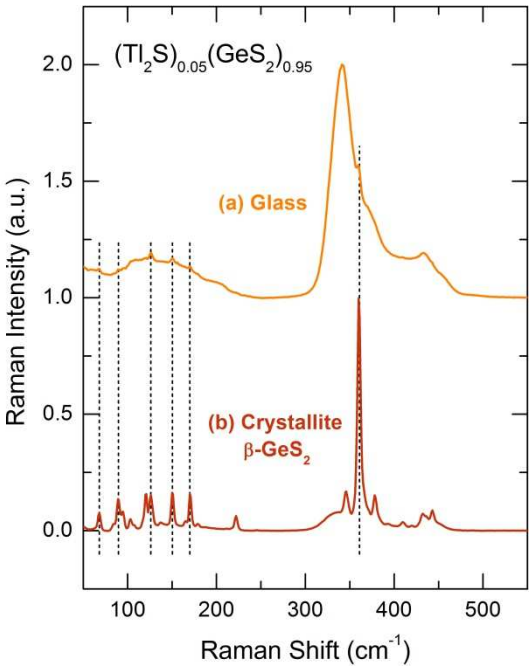

Figure 5. Raman spectra of (a) $(Tl_2S)_{0.05}(GeS_2)_{0.95}$ glass and (b) crystalline impurities of high-temperature β-GeS_2, found on the surface of the $x = 0.05$ sample.

Experimental Raman spectra of the $(Tl_2S)_x(GeS_2)_{1-x}$ glasses are shown in Fig. 6. Two contrasting composition trends are observed for semiconducting ($x \leq 0.3$) and ion-conducting ($x > 0.3$) glasses, consistent with composition limits of the $(Tl_2S)_x(GeS_2)_{1-x}$ compounds [13].

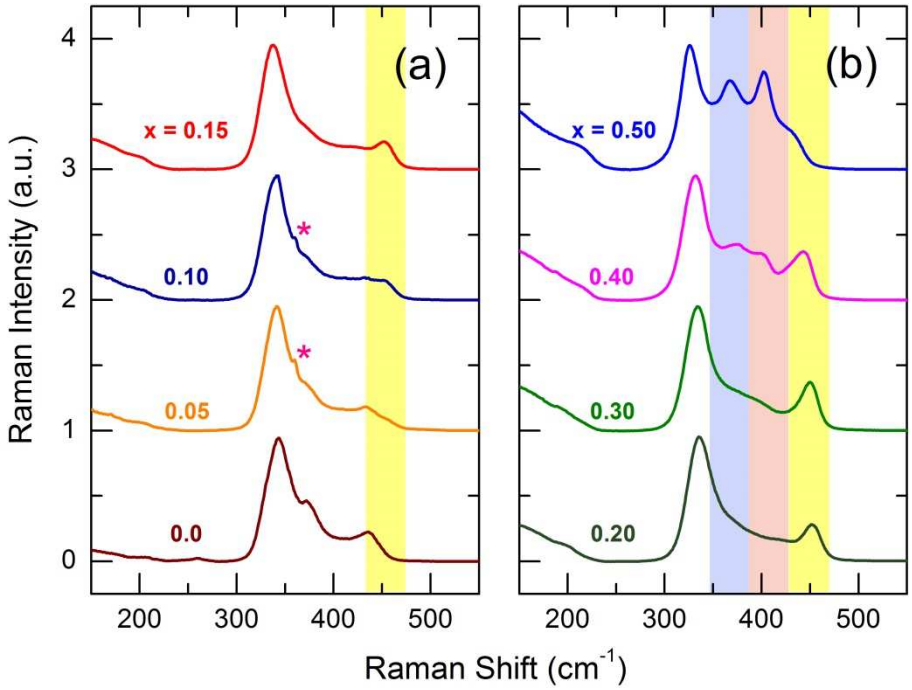

Figure 6. Experimental Raman spectra of the $(Tl_2S)_x(GeS_2)_{1-x}$ glasses: (a) $0 \leq x \leq 0.15$ and (b) $0.2 \leq x \leq 0.5$. Characteristic spectral features related to adamantane-like units, corner-sharing CS-Ge_mS_n oligomers and ES-Ge_2S_6 dimers are highlighted in yellow, red and blue, respectively. The A_1 mode of high-temperature β-GeS_2 crystalline impurities at ≈361 cm^{-1}, observed in thallium-poor glasses (x = 0.05 and 0.10), is indicated by a magenta star.

At $x \leq 0.3$, the Raman spectrum of g-GeS_2 exhibits characteristic changes. (i) One observes the appearance and growth of a new 450 cm^{-1} mode, similar to the A_1 mode in Ge_4S_{10} adamantane units corresponding to in-phase Ge-S_t stretching. (ii) The A_1 symmetric Ge-S stretching mode in CS-$GeS_{4/2}$ tetrahedra at 344 cm^{-1} shifts to lower frequencies. (iii) The A_1 symmetric (372 cm^{-1}) and F_2 asymmetric (435 cm^{-1}) modes in ES-$GeS_{4/2}$ tetrahedra disappear with increasing x. The above changes indicate a gradual transformation of the continuous g-GeS_2 network into a fragmented disordered structure consisting of isolated adamantane-like units and connecting Tl species. Similar trend was reported earlier for alkali thiogermanate glasses [28,34].

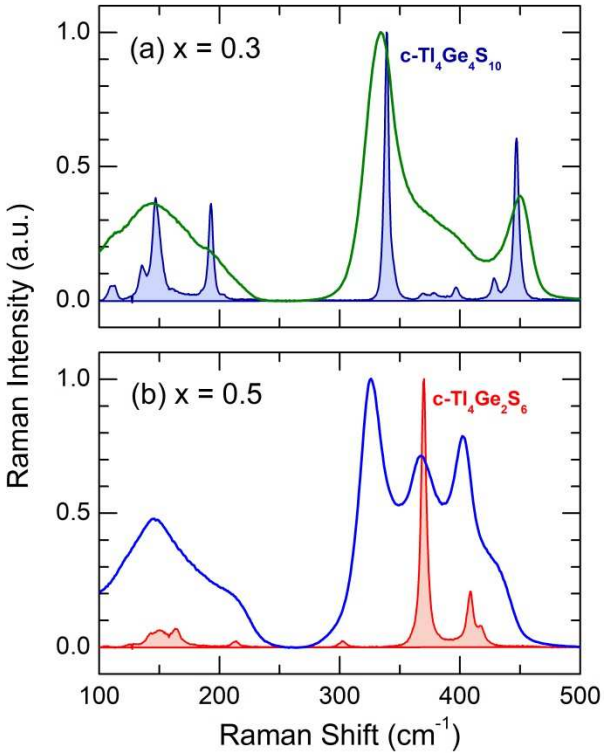

Figure 7. Experimental Raman spectra of $(Tl_2S)_x(GeS_2)_{1-x}$ glasses in comparison with respective crystalline compounds: (a) x = 0.3 and c-$Tl_4Ge_4S_{10}$ (x = ⅓); (b) x = 0.5 and c-$Tl_4Ge_2S_6$ ($x = \frac{1}{2}$).

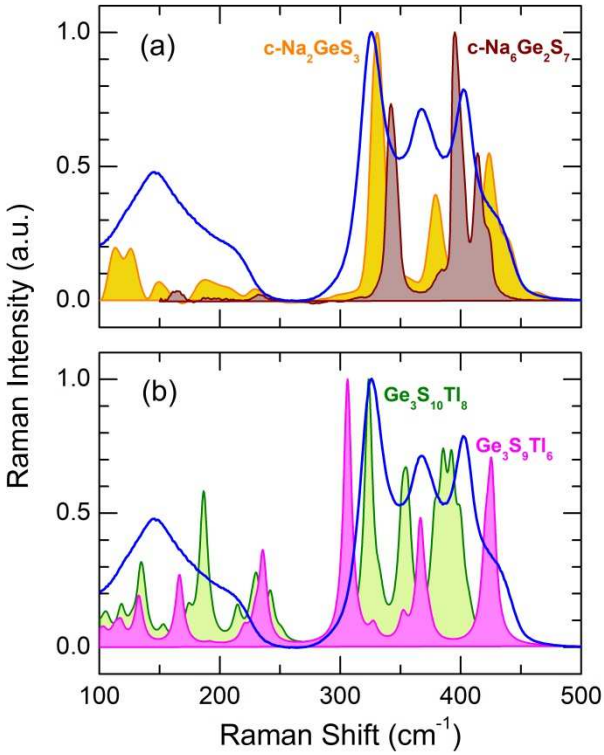

Figure 8. Experimental Raman spectra of the x = 0.5 glass and (a) crystalline references c-Na_2GeS_3 and c-$Na_6Ge_2S_7$ [34]; (b) DFT Raman spectra of $Ge_3S_{10}Tl_8$ and $Ge_3S_9Tl_6$ clusters.

The x = 0.3 glass has a nearly identical composition to monoclinic $Tl_4Ge_4S_{10}$ (x = ⅓) and shows a similar Raman spectrum with one important difference, a significant population of Ge-S stretching modes between 350 and 420 cm^{-1}, Fig. 7(a). Changes in this spectral region become predominant for ion-conducting $(Tl_2S)_x(GeS_2)_{1-x}$ glasses at $x > 0.3$.

The Tl-rich x = 0.5 glass has the same composition as triclinic $Tl_4Ge_2S_6$ ($x = \frac{1}{2}$). Nevertheless, the two materials exhibit quite different Raman spectra, Fig. 7(b). The A_1 breathing mode of ES-Ge_2S_6 dimers at 370 cm^{-1} is present in the ion-conducting glasses, Fig. 6(b). However, this mode is not the most intense even for the x = 0.5 vitreous alloy, in contrast to its crystalline counterpart. The A_1 in-phase breathing of corner-sharing tetrahedral

units at 325 cm^{-1} remains the predominant spectral feature for the ion-conducting $(Tl_2S)_x(GeS_2)_{1-x}$ glasses. In other words, the structural motif of triclinic $Tl_4Ge_2S_6$, ES-Ge_2S_6 dimers, does not determine the local and intermediate-range order of Tl-rich glasses at $x > 0.3$. In addition, the second most intense feature at 400 cm^{-1} ($x = 0.5$) does not have the crystalline analogue in the Tl_2S-GeS_2 system, Fig. 2(a), suggesting a new bonding pattern for the ion-conducting glasses.

The fast ion-conducting Na_2S-GeS_2 system [34] allows the structural puzzle to be solved. Two crystalline compounds in this system, monoclinic Na_2GeS_3, space group $P2_1/c$ [33], and monoclinic $Na_6Ge_2S_7$, space group $C2/c$ [46], reveal different crystal structures compared to heavy alkali and thallium thiogermanates, discussed previously. The Raman spectra of these two monoclinic crystals [34] show some resemblances with unidentified spectral features in the Tl-rich thiogermanate glasses, Fig. 8(a).

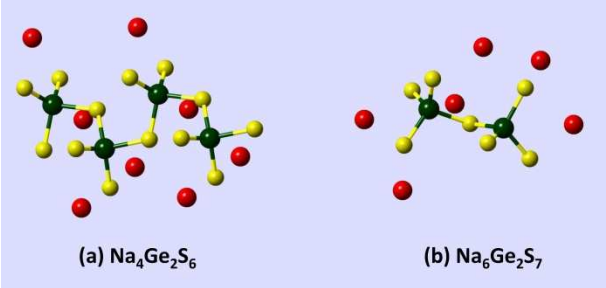

Figure 9. The crystal structure of (a) monoclinic Na_2GeS_3 = $Na_4Ge_2S_6$, space group $P2_1/c$ [33], and (b) monoclinic $Na_6Ge_2S_7$, space group $C2/c$ [46].

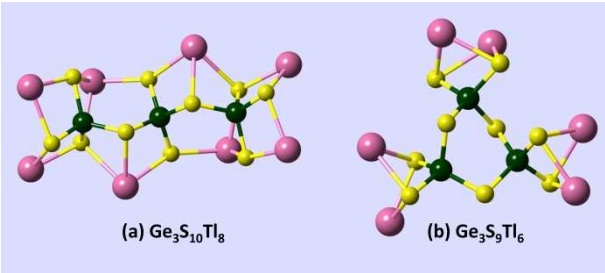

Figure 10. The optimized structure of corner-sharing oligomeric clusters used for DFT modelling: (a) CS-$Ge_3S_{10}Tl_8$ trimer, and (b) CS-$Ge_3S_9Tl_6$ ring.

The two Na_2S-GeS_2 crystals consist of CS-$GeS_{4/2}$ tetrahedra (Fig. 9). In monoclinic Na_2GeS_3, the tetrahedra form infinite chains, $(CS\text{-}GeS_2S_{2/2})_\infty$, while $Na_6Ge_2S_7$ is built up by CS-Ge_2S_7 dimers. The two Ge-S structural motifs are connected by sodium species. The stretching frequencies of the A_1 in-phase breathing modes of CS-units for the two crystals show a blue shift, +6 cm^{-1} (Na_2GeS_3) or +17 cm^{-1} ($Na_6Ge_2S_7$), consistent with a smaller average oscillator mass in sodium crystals compared to thallium thiogermanate glasses. The symmetric and asymmetric Ge-S_t stretching frequencies involving terminal sulfur are matching better a poorly resolved bimodal high-frequency feature at 400 and 435 cm^{-1} for the $x = 0.5$ glass, Fig. 8(a). A preliminary DFT modelling of several oligomeric CS-$Ge_mS_nTl_k$ clusters, Fig. 10, shows a general agreement with the experimental Raman spectra, Fig. 8(b), but needs to be continue to precise the exact stoichiometry of oligomeric CS-units.

4. Conclusions

The experimental Raman spectra of the known crystalline compounds in the Tl_2S-GeS_2 system are consistent with the crystal structure and DFT modelling of the respective Tl-Ge-S

clusters, representing structural motifs in c-$Tl_4Ge_4S_{10}$, c-$Tl_4Ge_2S_6$, and c-Tl_4GeS_4. Structural motifs in $(Tl_2S)_x(GeS_2)_{1-x}$ glasses, where $0 \leq x \leq 0.5$, are reminiscent of respective Tl_2S-GeS_2 crystals and, more specifically, of thallium-poor monoclinic $Tl_4Ge_4S_{10}$ (x = 1/3) and equimolar triclinic $Tl_4Ge_2S_6$ (x = 1/2). The Raman spectra of the $(Tl_2S)_x(GeS_2)_{1-x}$ glasses can be divided into two groups: (1) semiconducting glasses at $x \leq 0.3$, and (2) ion-conducting vitreous alloys at $x > 0.3$. At $x \leq 0.3$, the continuous g-GeS_2 network is transformed into a fragmented structure consisting of adamantane-like units Ge_4S_{10}, related to $Tl_4Ge_4S_{10}$, held together by thallium species. In the ion-conducting composition domain at $x > 0.3$ takes place further fragmentation of tetrahedral tetramers Ge_4S_{10} into ES-Ge_2S_6 dimers, as in $Tl_4Ge_2S_6$. However, the glasses at $x > 0.3$ consists also of small CS-oligomers, i.e., CS-Ge_2S_7 dimers or CS-Ge_3S_{10} trimers, absent in the Tl_2S-GeS_2 crystals but present in light alkali analogues, i.e., monoclinic $Na_6Ge_2S_7$.

Acknowledgments

This work was supported by the Région Hauts de France and the Ministère de l'Enseignement Supérieur et de la Recherche (CPER Climibio) as well as by the European Fund for Regional Economic Development. The DFT simulations were carried out using the CALCULCO computing platform, supported by SCoSI/ULCO (Service Commun du Système d'Information de l'Université du Littoral Côte d'Opale).

Bibliographie

[1] M.R. Riley, P. Lucas, D. Le Coq, C. Juncker, D.E. Boesewetter, J.L. Collier, D.M. DeRosa, M.E. Katterman, C. Boussard-Ple´del, B. Bureau, Lung Cell Fiber Evanescent Wave Spectroscopic Biosensing of Inhalation Health Hazards, Biotechnol. Bioeng. 95 (2006) 599-612.

[2] J.S. McCloy, B.J. Riley, D.A. Pierce, B.R. Johnson, A. Qiao, Infrared-transmitting glass–ceramics: a review, Proc. SPIE. 8708 (2013) 87080N.

[3] Yu.G. Mourzina, M.J. Schöning, J. Schubert, W. Zander, A.V. Legin, Yu.G. Vlasov, H. Lüth, Copper, cadmium and thallium thin film sensors based on chalcogenide glasses, Anal. Chim. Acta 433 (2001) 103-110.

[4] M. Milochova, M. Kassem, E. Bychkov, Chalcogenide glass chemical sensor for cadmium detection in industrial environment, ECS Transactions 50 (2012) 357-362.

[5] Yu. Ermolenko, D. Kalyagin, I. Alekseev, E. Bychkov, V. Kolodnikov, N. Melnikova, I. Murin, Yu. Mourzina, Yu. Vlasov, New membrane material for thallium (I)-selective sensors based on arsenic sulfide glasses, Sens. Actuators B 207 (2015) 940-944.

[6] B. Alrifai, M. Kassem, J. Toufaily, M. Bokova, E. Bychkov, Pb^{2+} potentiometric chemical sensors based on lead and silver doped thioaresenate glasses, Solid State Sciences 131 (2022) 106955.

[7] E. Robinel, B. Carette, M. Ribes, Silver sulphide based glasses (I). Glass forming regions, structure and ionic conduction of glasses in GeS_2-Ag_2S and GeS_2-Ag_2S-AgI systems, J. Non-Cryst. Solids 57 (1983) 49-58.

[8] M. Bokova, I. Alekseev, D. Kalyagin, V. Tsegelnik, Y. Ermolenko, E. Bychkov, ^{204}Tl

tracer diffusion and conductivity in thallium thiogermanate glasses, Solid State Ionics 253 (2013) 101-109.

[9] M. Kitao, M. Senda, Y. Takano, S. Yamada, Effect of Tl additive on conductivity and absorption coefficient in glassy As_2Se_3, J Non-Cryst Solids 127 (1991) 36–43.

[10] M. Bokova, I. Alekseev, E. Bychkov, Mixed cation effect in Ag_2S-Tl_2S-GeS-GeS_2 glasses: Conductivity and tracer diffusion studies, Solid State Ionics 273 (2015) 55–58.

[11] C. Rau, P. Armand, A. Pradel, C.P.E. Varsamis, E.I. Kamitsos, D. Granier, A. Ibanez, E. Philippot, Mixed cation effect in chalcogenide glasses Rb_2S-Ag_2S-GeS_2, Phys. Rev. B 63 (2001) 184204.

[12] M. Kassem, I. Alekseev, M. Bokova, D. Le Coq, E. Bychkov, Ionic-to-Electronic Conductivity Crossover in CdTe-AgI-As_2Te_3 Glasses: An ^{110m}Ag Tracer Diffusion Study, J. Phys. Chem. B 122 (2018) 4179-4186.

[13] M. Bokova, A. Paraskiva, M. Kassem, I. Alekseev, E. Bychkov, Tl_2S-GeS-GeS_2 system: glass formation, macroscopic properties, and charge transport, J. Alloys Compd. 777 (2019) 902-914.

[14] X.F. Wang, S.X. Gu, J.G. Yu, X.J. Zhaoa, H.Z. Tao, Structural investigations of GeS_2–Ga_2S_3–CdS chalcogenide glasses using Raman spectroscopy, Solid State Communications 130 (2004) 459–464.

[15] R.M. Almeida, H. Nasu, J. Heo, J.D. Mackenzie, Identification of non-bridging sulphur atoms in GeS_2-Tl_2S glasses J. Mater. Sci. Lett. 6 (1987) 701–704.

[16] G. Qu, C. Lin, Z. Li, S. Zhai, S. Gu, H. Tao, T. Xu, Glass formation and physical properties of chalcogenide glasses in Ge–S–Pb system, Infrared Physics & Technology 63 (2014) 184–188.

[17] H. Guo, Y. Zhai, H. Tao, G. Dong, X. Zhao, Structure and properties of GeS_2–Ga_2S_3–CdI_2 chalcohalide glasses, Mater. Sci. Eng. B 138 (2007) 235–240.

[18] S. Barnier, M. Guittard, C. Julien, Glass formation and structural studies of chaicogenide glasses in the CdS-Ga_2S_3-GeS_2 system, Mater. Sci. Eng. B 7 (1990) 209-214.

[19] M. Bokova, A. Paraskiva, M. Kassem, E. Bychkov, Mixed cation Ag_2S-Tl_2S-GeS_2 glasses: macroscopic properties and Raman scattering studies, J. Phys.: Condens. Matter 32 (2020) 264004.

[20] R. Zaiter, M. Kassem, M. Bokova, A. Cuisset, E. Bychkov, Mercury Thiogermanate Glasses HgS-GeS_2: Vibrational, Macroscopic, and Electric Properties, J. Phys. Chem. B 124 (2020) 7075–7085.

[21] G. Eulenberger, Die Kristallstruktur des Thallium(I)thiogermanats $Tl_4Ge_4S_{10}$, Acta Cryst. B 32 (1976) 3059-3063.

[22] G. Eulenberger, Tetrathalllum(1)-di-/m-thio-tetrathiodigermanat, Acta Cryst. B 34 (1978) 2614-2616.

[23] G. Eulenberger, Die Kristallstruktur des Thallium(I)thiogermanats Tl_4GeS_4, Z. Kristallogr. 145 (1977) 427-436.

[24] G. Dittmar, H. Schäfer, Die Kristallstruktur von H.T.-GeS_2, Acta Cryst. B31 (1975) 2060-2064.

[25] G. Dittmar, H. Schäfer, Die Kristallstruktur von L.T.-GeS_2, Acta Cryst. B 32 (1976) 1188-1192.

[26] K. O. Klepp, M. Zeitlinger, Crystal structure of tetracesium decasulfidotetragermanate, $Cs_4Ge_4S_{10}$, Z. Kristallogr. New Crystal Structures, 215 (1) (2000) 7-8.

[27] C. Köster, A. Lindemann, J. Kuchinke, C. Mück-Lichtenfeld, B. Krebs, Syntheses,

crystal structures and vibrational properties of $Rb_4Si_4S_{10}$ and $Rb_4Si_4Se_{10}$, Solid State Sciences 4 (2002) 641–650.

[28] C.R. Nelson, S. Poling, S.W. Martin, Synthesis and characterisation of potassium, rubidium, and cesium thiogermanate glasses, J. Non-Cryst. Solids 337 (2004) 78–85.

[29] Frisch, M. J.; Trucks, G. W.; Schlegel, H. B.; Scuseria, G. E.; Robb, M. A.; Cheeseman, J. R.; Scalmani, G.; Barone, V.; Petersson, G. A.; Nakatsuji, H.; Li, X.; Caricato, M.; Marenich, A. V.; Bloino, J.; Janesko, B. G.; Gomperts, R.; Mennucci, B.; Hratchian, H. P.; Ortiz, J. V.; Izmaylov, A. F.; Sonnenberg, J. L.; Williams-Young, D.; Ding, F.; Lipparini, F.; Egidi, F.; Goings, J.; Peng, B.; Petrone, A.; Henderson, T.; Ranasinghe, D.; Zakrzewski, V. G.; Gao, J.; Rega, N.; Zheng, G.; Liang, W.; Hada, M.; Ehara, M.; Toyota, K.; Fukuda, R.; Hasegawa, J.; Ishida, M.; Nakajima, T.; Honda, Y.; Kitao, O.; Nakai, H.; Vreven, T.; Throssell, K.; Montgomery, J. A.; Peralta, J. E.; Ogliaro, F.; Bearpark, M. J.; Heyd, J. J.; Brothers, E. N.; Kudin, K. N.; Staroverov, V. N.; Keith, T. A.; Kobayashi, R.; Normand, J.; Raghavachari, K.; Rendell, A. P.; Burant, J. C.; Iyengar, S. S.; Tomasi, J.; Cossi, M.; Millam, J. M.; Klene, M.; Adamo, C.; Cammi, R.; Ochterski, J. W.; Martin, R. L.; Morokuma, K.; Farkas, O.; Foresman, J. B.; Fox, D. J. Gaussian 16, revision B.01; Gaussian, Inc.: Wallingford, CT, 2016.

[30] A.D. Becke, Density-functional thermochemistry. III. The role of exact exchange, J. Chem Phys. 98 (1993) 5648-5653.

[31] C. Lee, W. Yang, R.G. Parr, Development of the Colle-Salvetti correlation-energy formula into a functional of the electron density, Phys Rev B Condens Matter Phys. 37 (1988) 785-789.

[32] A. Cuisset, F. Hindle, J. Laureyns, E. Bychkov, Structural analysis of xCsCl(1-x)Ga2S3 glasses by means of DFT calculations and Raman spectroscopy, J. Raman Spectrosc. 41 (2010) 1050-1058.

[33] J. Olivier Fourcade, E. Philippot, M. Ribes, M. Maurin, Structure cristalline du thiogermanate de sodium Na_2GeS_3, C. R. Acad. Sci. Paris C274 (1972) 1185-1187.

[34] B. Barrau, M. Ribes, M. Maurin, A. Kone, J-L. Souquet, Glass formation, structure and ionic conduction in the Na_2S-GeS_2 system, J. Non-Cryst. Solids 37 (1980) 1-14.

[35] P. Masselin, D. Le Coq, A. Cuisset, E. Bychkov, Spatially resolved Raman analysis of laser induced refractive index variation in chalcogenide glass, Opt. Mater. Express 2 (2012) 1768-1775.

[36] I. Petri, P.S. Salmon, A neutron diffraction study of glassy GeS_2, J. Non-Cryst. Solids 293-295 (2001) 169-174.

[37] E. Bychkov, M. Miloshova, D.L. Price, C.J. Benmore, A. Lorriaux, Short, intermediate and mesoscopic range order in sulfur-rich binary glasses, J. Non-Cryst. Solids 352 (2006) 63–70.

[38] A. Bytchkov, G.J. Cuello, S. Kohara, C.J. Benmore, D.L. Price, E. Bychkov, Unravelling the atomic structure of Ge-rich sulphide glasses, Phys. Chem. Chem. Phys. 15 (2013) 8487-8494.

[39] J.E. Griffiths, J.C. Phillips, G.P. Espinosa, J.P. Remeika, P.M. Bridenbaugh, Assignment of the companion A1c line in $Ge_x(S, Se)_{1-x}$ glasses, Phys. Stat. Solidi B 122 (1984) K11–K15.

[40] S. Sugai, Stochastic random network model in Ge and Si chalcogenide glasses, Phys. Rev. B 35 (1987) 1345–1361.

[41] K. Inoue, O. Matsuda, K. Murase, Raman spectra of tetrahedral vibrations in crystalline germanium dichalcogenides, GeS_2 and $GeSe_2$, in high and low temperature forms, Solid

State Commun. 79 (1991) 905–910.

[42] G. Lucovsky, F.L. Galeener, R.C. Keezer, R.H. Geils, H.A. Six, Structural interpretation of the infrared and Raman spectra of glasses in the alloy system $Ge_{1-x}S_x$, Phys. Rev. B 10 (1974) 5134–5146.

[43] I.P. Kotsalas, C. Raptis, High-temperature structural phase transitions of Ge_xS_{1-x} alloys studied by Raman spectroscopy, Phys. Rev. B 64 (2001) 125210.

[44] K. Jackson, A. Briley, S. Grossman, D.V. Porezag, M.R. Pederson, Raman-active modes of a–$GeSe_2$ and a–GeS_2: a first-principles study, Phys. Rev. B 60 (1999) R14985–R14989.

[45] S. Blaineau, P. Jund, Vibrational signature of broken chemical order in a GeS_2 glass: A molecular dynamics simulation, Phys. Rev. B 69 (2004) 064201.

[46] J-C. Jumas, J. Olivier Fourcade, F. Vermot-Gaud-Daniel, M. Ribes, E. Philippot, M. Maurin, Etude structurale de thiocomposés à groupements anioniques de type -pyro-, $Na_6X_2S_7$ (X = Ge, Sn) et $Ba_3Sn_2S_7$, Rev. Chim. Miner. 11 (1974) 13-26.